RSC Advances

ROYAL SOCIETY OF CHEMISTRY

www.rsc.org/advances

Graphical abstract for

The induction of poly(vinylidene fluoride) electroactive phase by modified anodic aluminum oxide template nanopores surface

Chao Fu,[ab] Xuemei Wang,[a] Xiang Shi,[ab] and Xianghai Ran,[a*]

[a] Lab of Polymer Composites Engineering, Changchun Institute of Applied Chemistry,Chinese Academy of Sciences, Changchun 130022, China.

E-mail: ranxh@ciac.jl.cn;

Fax: +86 431 85262424; Tel: +86 431 85262677

[b] University of Chinese Academy of Sciences, Beijing 100049, China

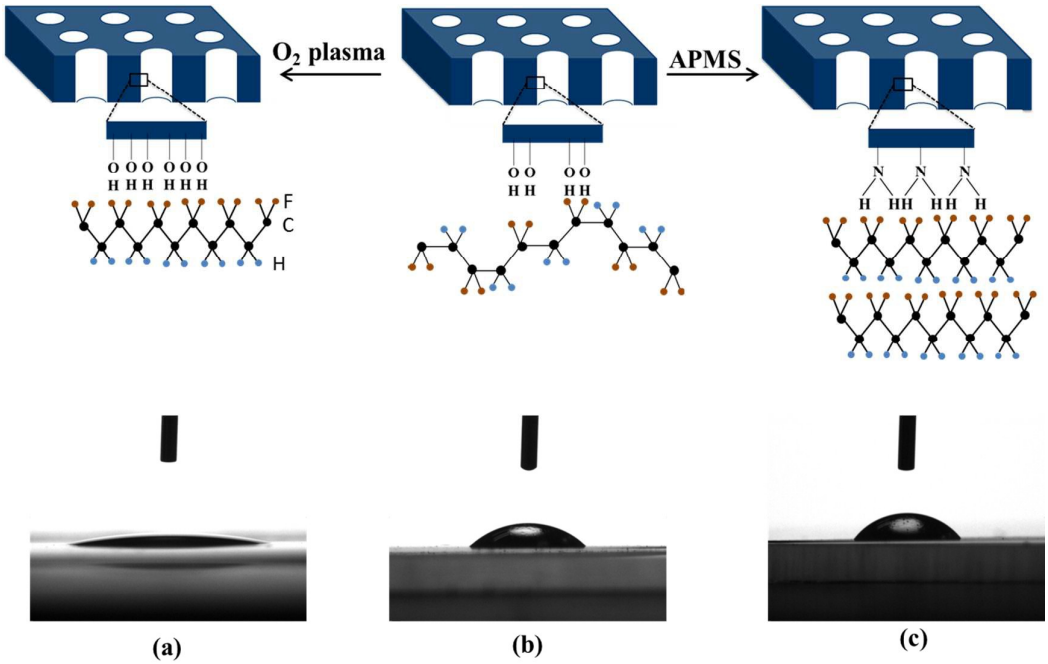

Figure 1 The contact angle measurements of water droplet on the surface of oxygen plasma treatment (a), pristine (b) and APMS modified (c) AAO templates and corresponding schematic diagram of the polar phase formation.

Cite this: DOI: 10.1039/c0xx00000x

www.rsc.org/xxxxxx

ARTICLE TYPE

The induction of poly(vinylidene fluoride) electroactive phase by modified anodic aluminum oxide template nanopores surface

Chao Fu,[ab] Xuemei Wang,[a] Xiang Shi,[ab] and Xianghai Ran,[a*]

Received (in XXX, XXX) Xth XXXXXXXXX 20XX, Accepted Xth XXXXXXXXX 20XX

DOI: 10.1039/b000000x

Abstract

The desired electroactive β and γ phase of poly(vinylidene fluoride)(PVDF) nanostructures are rarely obtained through wetting anodic aluminum oxide (AAO) template method. Further and systematic studies on the corresponding induction mechanism are also lacking. Herein, we designed and fabricated the PVDF nanowires using solution wetting pristine and modified AAO templates method. The morphology and crystalline structure of PVDF nanowires were characterized by SEM and micro-FTIR respectively. Then, the induction mechanism was investigated by AFM, FTIR, TGA and contact angle measurement. It is found that the polarity of solvent and the surface hydroxyl groups on templates nanopores both have the induction effect on the polar phase. After the oxygen plasma treatment, the proportion of β phase of PVDF nanowires becomes higher although the total polar phase content remains the same. This is attributed to high polarity of nanopores surface and regular arrangement among hydroxyl groups. Polar phase content of PVDF nanowires increase from 40% prepared by the pristine template to 71% by the 3-aminopropyltrimethoxysilane (APMS) modified template. It can be explained that more interaction points and stronger interactions result in more electroactive phase.

Introduction

The PVDF homopolymer and its copolymer are most widely used piezoelectric polymer due to high piezoelectric coefficient, fast ferroelectric switch speed and high Curie temperature. However, the applicability and adaptability of piezoelectric polymer are greatly impeded by large ferroelectric loss. [1, 2] Ferroelectric domains can be physically confined by nanosized crystallites, where ferroelectric domain coupling is weak enough to result in a low coercive voltage. [3, 4] Actually, to fabricate the nanostructured polymer is an effective way to hit off the above mentioned drawback. Nowadays, emerged ways to acquire polymer one-dimensional (1D) nanostructures are wetting templates, [5-7] nanoimprint lithography, [8, 9] microphase-separated block copolymers [10, 11] and electrospinning [12, 13, 14] *etc*. Indeed, these methods open up the path for practical application of novel organic electronics, such as non-volatile memories, nanogenerators, nanosensors and nanoactuators. [15-19] Among these methods wetting the anodic aluminum oxide (AAO) templates is a low-cost, simple and effective way to obtain polymer one-dimensional nanostructures with uniform size.

PVDF presents polymorphism, which has three major crystalline phases: nonpolar α phase (TGTG), polar β phase (TTT) and γ phase ($T_3G^+T_3G^-$). [20] The nonpolar α phase is obtained in common processing conditions. Though polar β phase and γ phase display piezoelectricity, they are not easy to obtain due to their thermodynamic instability. [21] Moreover, β phase content has a profound influence on degree of polarization. The copolymer poly (vinylidene fluoride–trifluoroethylene) (P(VDF-TrFE)) crystallizes predominantly in the β phase due to steric factors. These P(VDF-TrFE) nanostructures therefore exhibit electroactive phase. [19, 22-26] While compared with P(VDF-TrFE), PVDF presents lower density, stronger dipole interactions, and more reactive synthesis character. [27] Therefore, it is significant to obtain the PVDF nanostructures with small ferroelectric domains size (low coercive voltage) as well as with high content of electroactive phase (high remnant polarization).

When PVDF melt infiltrated into AAO templates, the nonpolar α phase is obtained. [28, 29] While the PVDF pellets are dissolved in solvent with higher dipole moment and then the solution is cast onto a template, β and γ phase are derived. [30-33] Similar to other solution-based polymer processing methods, it is reasonable to expect that solution wetting has more controllable factors that may influence the electroactive phase content than melt wetting. However, little study has focused on the mechanism of electroactive phase induction effect with this method. Li *et al* reported that the surface hydroxyl groups stabilized the all-trans conformation of PVDF nanostructures in the condition of solution thus leading to the formation of β phase. [32] Kim *et al* investigated crystalline phases of PVDF nanostructures crystallized from mixed solvent with different ratios of dimethyl sulfoxide (DMSO) and acetone. They observed more β phase in solution with high volume ratio of DMSO, which shows high polarity. [33] Both of the above explanations may light up the way of improving the electroactive phase content. Herein, the underlying mechanism that electroactive phase of PVDF nanostructures crystallized from

solution in AAO templates is studied. The electroactive phase content is further increased by modifying AAO templates with oxygen plasma and APMS. In addition, the induction mechanism is researched.

Experiment

Fabrication of PVDF nanostructures

The AAO templates were placed in an oxygen plasma generator (ME-1, CAS) for 5 min then used immediately. The templates were immersed in a 0.1% (v/v) solution of APMS in methanol for 12 h under room temperature. After that the templates were washed by methanol several times and then dried at 120 °C for 4h. The one-end sealed AAO templates (pores size of 200 nm, depth of 50 μm, Nanjing XFNANO) were immersed in the solution of PVDF in DMF at 50 °C for a period of time to insure the completed infiltration. Afterwards, the templates were dried at a definite temperature under ambient conditions for 1 h then in vacuum oven for 10 h. The PVDF solution was dropped onto the two-end unsealed templates (pores size of 50 nm, depth of 50 μm, Nanjing XFNANO), and capillary force drive the solution infiltrate into the pores of templates. The drying process was same with the one-end sealed template. The residual films on the surface of templates were removed by a surgical blade and emery paper mechanically. Then plasma etch process was required to completely remove the residual polymer film.

Characterization

The AAO templates were etched off by 1 mol/L NaOH aqueous solution to release the nanowires. The morphology of PVDF nanostructures were observed with field emission scanning electron microscopy (SEM, XL-30). A PVDF film with protruding nanowires thin slice was observed using a transmission electron microscope (TEM, JEOL JEM-1011). The slice was embedded in epoxy resin. The specimen for TEM observations (50-70nm thickness) was prepared under cryogenic conditions using a Leica ultramicrotome. Thin slices for micro-FTIR analysis, were cut down under an optical microscope using a razor blade. The crystalline phase of nanostructures was verified by micro-FTIR (Bruker, IFS 66 V/S spectrometer in connection with a Bruker Hyperion 3000 microscope) in the transmission mode. The pristine and modified templates surfaces were examined by atomic force microscopy (AFM, SPI 3800/SPA 300HV) with tapping mode. The contact angle of 2μL water droplet deposited on the surface of AAO templates were measured on a video based contact angle measuring device (KRUSS, DSA30). The thermal properties of different AAO templates and PVDF nanowires filled in different templates were investigated by thermogravimetric analysis (TGA). TGA was carried out on a TA/DSC1 instrument in the nitrogen at a heating rate of 10 ºC/min from room temperature to 800ºC.

Result and discussion

Morphology and crystal structure of PVDF nanowires

Representative SEM micrographs of the obtained PVDF nanowires are shown in Fig. 1. The residual layer on top of the template is almost removed by mechanical polishing and plasma etching (Fig .1a). The wetting conditions, such as wetting temperature, wetting time and viscosity of solution, strongly influence the volume of liquid infiltration into nanochannels. [34] Under controlled wetting conditions, the solution infiltrates the template thoroughly. The sufficient infiltration time and proper temperature result in solid nanowires within both 50 and 200 nm templates. The wetting conditions related to the wetting degree do not affect the subsequent crystallization process. Fig. 1b-f displays that the fabricated PVDF nanowires effectively duplicate the size of template nanopores giving place to large aspect ratio nanowires when the solvent evaporates completely.

The micro-FTIR was used to further characterize crystalline phase of the PVDF nanowires. Micro-FTIR provides a simple and powerful approach for local analysis of material presenting different appearances under a microscope. [35] The TEM image and optical micrograph (inset) of the slice cross-section are shown in Fig. 2a. The nanowires may lean and break when cutting the TEM specimen. So the nanowires shown in TEM image are really short. The cross-section is composed of bulk film with thickness of 100 μm and nanowires with dimension of 50 μm approximately. The right side of the slice is opaque due to the light scattering behavior between the interfaces of numerous nanowires and the left side is transparent due to the isotropy of bulk. The solution concentration has a strong impact on flexibility of bulk film on the templates surface of solution wetting samples. The bulk films fabricated by the solution of 15wt% and 20wt% are most suitable for cutting slices and application. Because the lower concentration results in fragile bulk film whereas a higher concentration results in film with quite high toughness.

Fig. 2b displays the micro-FTIR spectra of nanowires crystallized at different temperature in pristine AAO template. When the wetted template is drying at 100 °C, the absorption peaks of nanowires at 613, 675, 763, 854, 975 and 1383 cm^{-1}

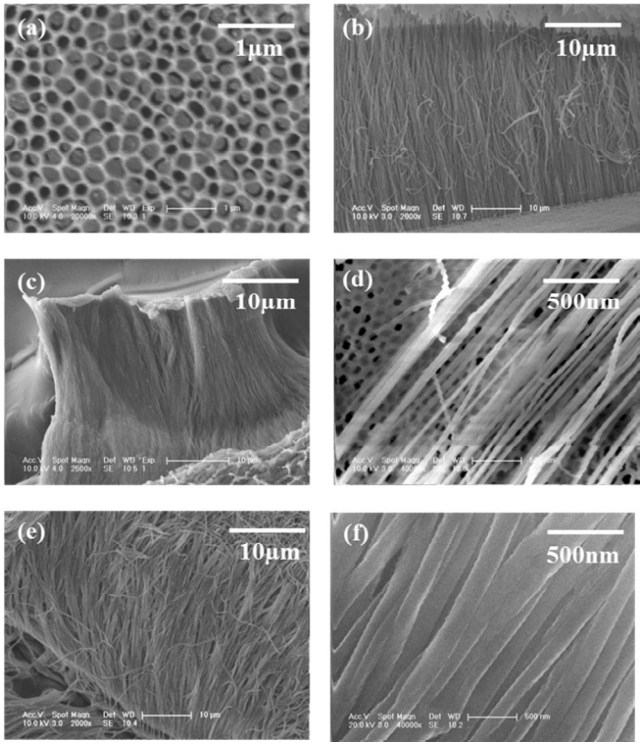

Figure 1 (a) pristine and (b) modified AAO templates with pore size of 200 nm; (c) top surface and (d) cross-section of nanowires within the template after removing the residual film; nanowires released from the templates with (e) and (f) 50 nm pores size; (g) and (h) 200 nm pores size.

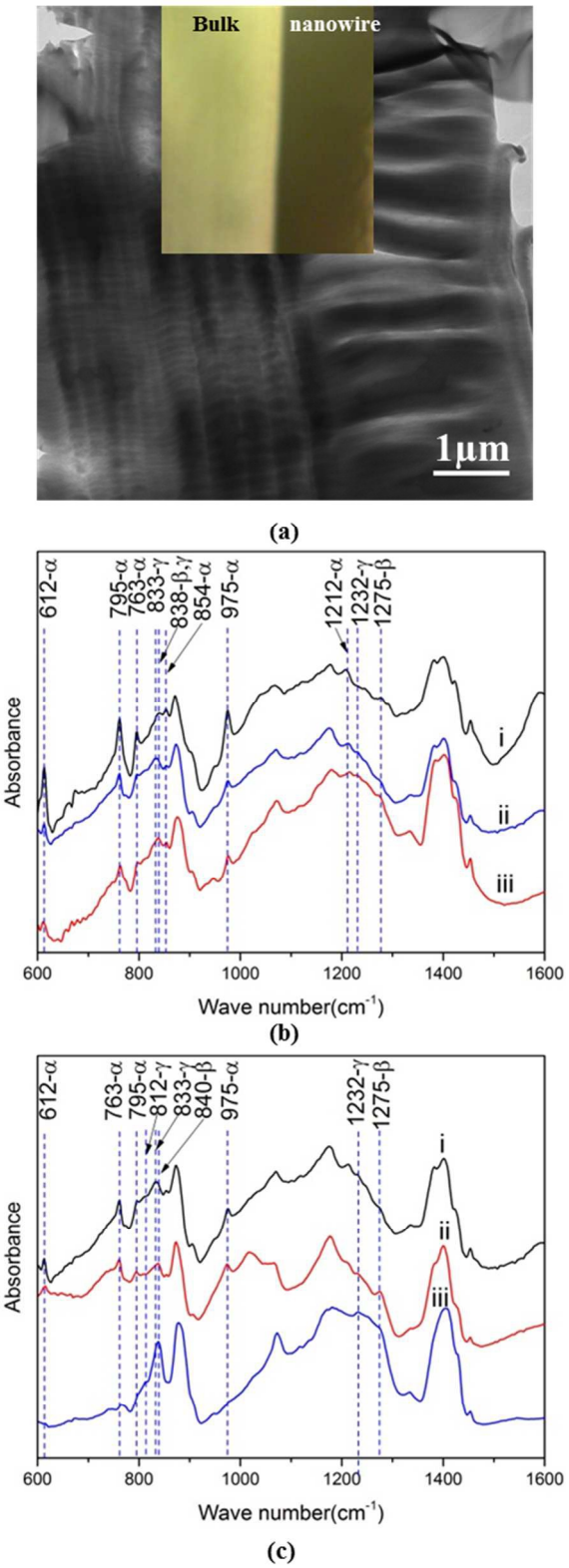

Figure 2 TEM image and optical micrograph (inset) of a PVDF film with protruding nanowires thin slice (a); micro-FTIR spectra of nanowires crystallized in the pristine AAO template at different condition: (i) 20wt% solution at 100 °C, (ii) 15wt% solution at 70 °C, (iii) 20wt% solution at 70 °C (b); and at 70 °C in different templates: (i) pristine, (ii) treated by oxygen plasma , (iii) modified by APMS (c).

corresponding to α phase are apparent and the intensity of peak at 838cm^{-1} assigned to overlapping of β and γ phase[36] is much lower. The sample drying at 70 °C shows much stronger absorption peak at 833 cm^{-1} that uniquely assigned to γ phase. It demonstrates that at higher temperature the solution-crystallized PVDF nanowires lead to more nonpolar α phase. This result is found to be consistent with previous studies for PVDF bulk films crystallized from solution. [21, 37-39]

As reported, polar phase content of solution crystallized bulk film is influenced by dry temperature, [40] rate of solvent evaporation, [41, 42] property of different solvent [43] and substrate [44] . At low temperature, intermolecular interactions between fluorine atoms of PVDF and polar moieties of N, N-dimethylacetamide (DMAc) become greater with the solvent polarity increasing. The interactions stabilize the all-trans conformation and promote more polar phase. [37] Much more solvent with higher dipole moment always promote a higher fraction of β phase. [33] The drying temperature can influence the polarity of solvent and solvent evaporation rate in the whole crystallization process. However, the solution concentration may only affect the solvent evaporation rate at the latter stage of crystallization process. [42] But the nucleation rate associated with different crystal phase nucleation is influenced by evaporation rate of initial stage. As a consequence, the solution concentration has a slight influence on solvent evaporation rate thus the crystal phase content. It is observed that the nanowires fabricated by solution of 15wt% and 20wt% drying at same temperature show almost same polar phase content (Fig. 1b). This implies that the effect of drying temperature is stronger than solution concentration. So we may conclude that lower drying temperature with increased polarity of solvent can effectively induce polar phase of PVDF nanowires. It also demonstrates that the induction effect of polar solvent cannot be ignored. Much lower temperature may result in slower mobility of polymer chain and more TG^+ or TG^- conformation defects. Therefore more γ phase is formed which is consist with the observations of García-Gutiérrez. [31]

In this work, the crystallization of PVDF electroactive phase is enhanced by modifying the templates nanopores surface with oxygen plasma and APMS as shown in Fig. 2c. At given crystallization condition, within the pristine and modified templates the crystalline phase content varies. After the oxygen plasma treatment, the spectrum of nanowires appears peak at 840 cm^{-1} and shows stronger intensity of peak at 1275 cm^{-1} assigned to β phase, although there is no change in the total amount of polar phase. The TG^+ or TG^- defects in the all-trans conformation of PVDF chains are decreased by modifying the templates with oxygen plasma, therefore lead to more β phase. Modifying the AAO templates with APMS leads to an increased proportion of polar crystalline phase. As shown in the spectra, the intensity of

Polar phase relative content of samples crystallized at different conditions

Samples crystallized at different conditions	F(p)(%)
20wt%-100°C-P	32.4
15wt%-70°C-P	39.9
20wt%-70°C-P	40.5
20wt%-70°C-OM	40.2
20wt%-70°C-AM	71.3

[a] solution concentration-drying temperature-template (P-pristine, OM-oxygen plasma modified, AM-APMS modified)

characteristic peak at 763 cm^{-1} ascribed to α phase is quite low and other peaks assigned to α phase disappeared. The main peak at 840 cm^{-1} assigned to β phase and shoulder peak at 812 cm^{-1} assigned to γ phase are obvious. It can be concluded that AAO templates functionalised with APMS increase the polar phase content of PVDF nanowires significantly. Therefore we provide a new method to improve the piezoelectricity of PVDF nanostructures. The polar phase relative content F(p) of samples crystallized from different conditions is determined from the FTIR spectra based on the following equation,

$$F(p) = \frac{A_p}{1.26A_n + A_p} \times 100\%$$

where A_n and A_p represent the absorbance of nonpolar phase characteristic peak at 763 cm^{-1} and polar phase characteristic peak at 833 or 840 cm^{-1}, respectively. [45] The results for different samples are summarized in Table 1 in detail.

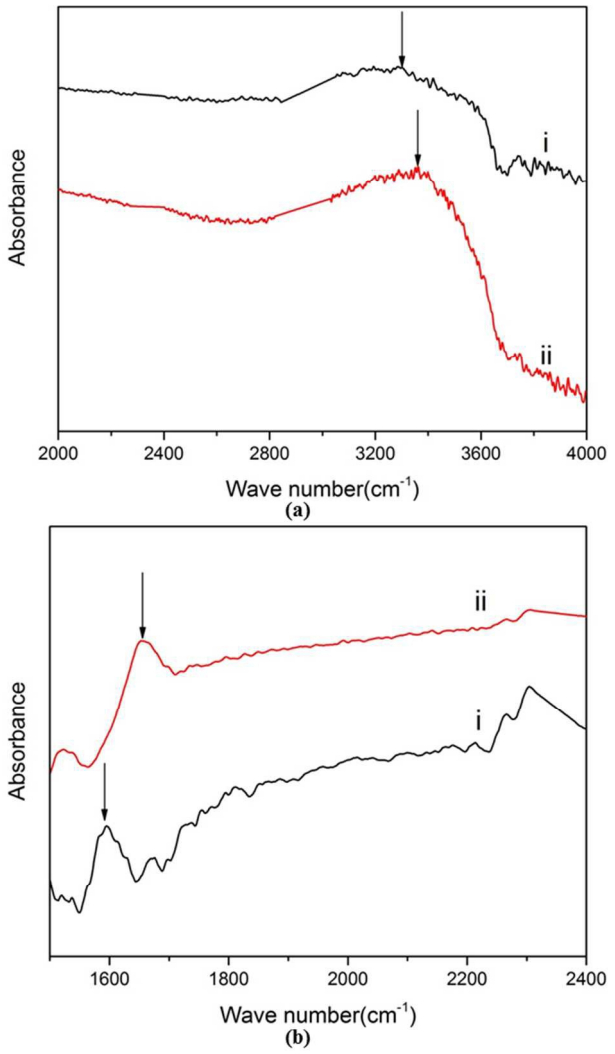

Figure 3 FTIR spectra of (a) bare (i) and PVDF nanowires filled (ii) pristine AAO template; (b) APMS modified templates (i) and PVDF nanowires filled in (ii) subtracted the vibration intensity of pristine template.

The mechanism of inducing electroactive phase PVDF nanostructures by modified AAO templates

Due to the difference between bulk and surface coordination numbers of aluminum ions, AAO templates surface are preferentially terminated by hydroxyl groups. [46] Fig. 3a shows the FTIR spectra of AAO templates with obvious vibration peak at 3300-3400cm^{-1} attributed to the stretching of the surface O-H groups. When PVDF nanowires fill in the template nanopores, the absorption band become stronger and slightly shift to lower frequency, suggesting that O-H bond is stretched by the interaction between PVDF chains and hydroxyl groups. The hydrogen bonds forming between the surface hydroxyl groups and fluorine atoms of PVDF molecule chains restrict the PVDF chains rotation and stabilize the all-trans conformation when molecule chains nucleate and fold into crystals. The conformation of the polymer chains within the crystal is that of the lowest possible energy. [47] As for PVDF, the helical α-conformation is more thermodynamics favor than all-trans β-conformation in general condition. [48, 49] The interactions between template surface functional groups and PVDF chains reduce the molecule potential to form β phase crystals. The surface-induction nucleation effect contributes to the polar phase of PVDF nanowires.

The AFM images that show the topography of pristine and modified templates are displayed in Fig. 4(a)-(c). The average RMS surface roughness values of the pristine, oxygen plasma treatment, and APMS modified AAO templates are 4.53 nm, 3.85 nm, 4.88 nm, respectively. The O_2 plasma treatment renders the dense surface of templates into sparse morphology with small grains (Fig 4a). As the plasma engraves the surface particles, it influences the microcrystalline exhibited in the phase images (Fig. S2a). The change in topography and microstructure of Al_2O_3 surface plausibly results in an oxygen vacancy-rich surface. [50] Thereby, oxygen plasma treatment can effectively increase the number of negatively charged OH^- and O^{2-} groups on the surface of the Al_2O_3 surface. [51, 52] Since it is known that the presence of OH^- and O^{2-} groups on a substrate surface contribute to attractive interactions between water molecules and the surface. [53] The water drop contact angle measurements (Fig. 5a) demonstrate that the surface of AAO template modified by oxygen plasma is more hydrophilic than the pristine one. Since it is known that more hydrophilic surface shows higher polarity. After the O_2 plasma treatment, the high polarity surface template reinforces the absorption between the templates nanopores surface and PVDF molecules. The TG^+ and TG^- conformation defects reduce dramatically due to the regular arrangement among hydroxyl groups. So oxygen plasma treated AAO templates give a higher content of β phase, though the total amount of polar phase remains the same.

Silanization has been demonstrated an effective and flexible method for changing the wetting and adsorption properties of AAO templates. [54] The aminosilane coupling agents can readily react with OH groups on alumina pores surfaces, resulting in amino derivatized nanopores wall. [55] The covalent attachment of the aminolsilane to the nanopores surface is identified (Fig. S1). APMS functionalized template is slightly rougher with RMS values of 4.88 nm compared to pristine one. Furthermore, the nanopores appear to be smaller on the APMS functionalised template (Fig. 4c, e), suggesting formation of aminolsilane layers

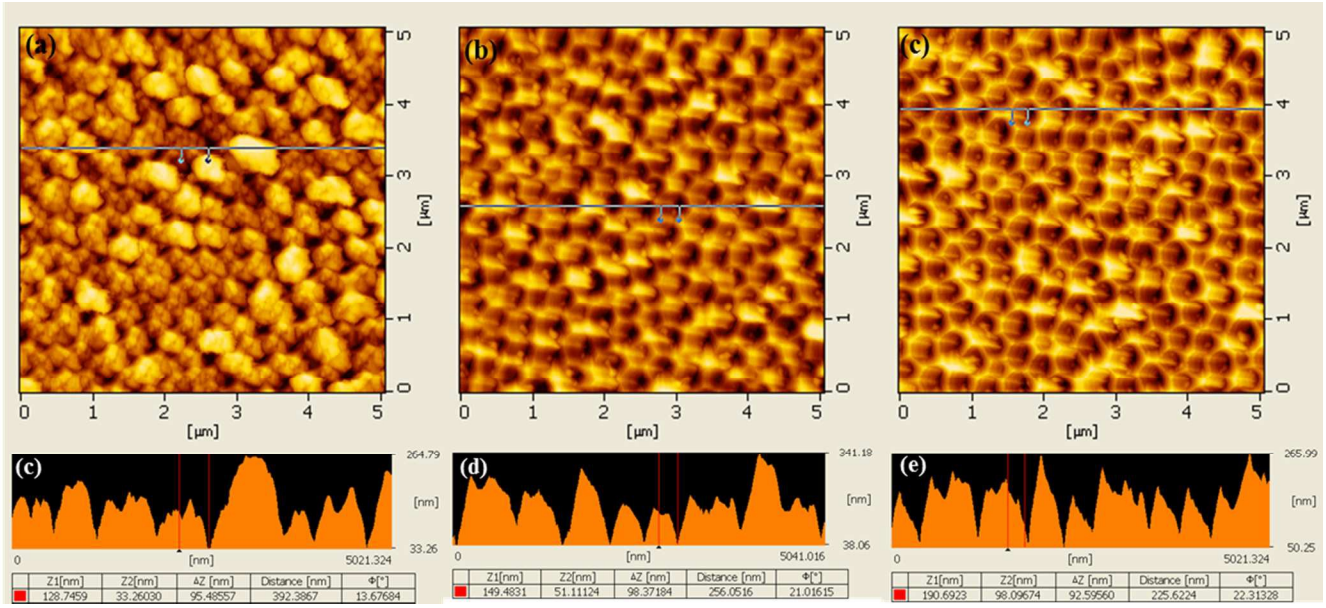

Figure 4 AFM topography image and cross-section along the blue line in the topography image of oxygen plasma treatment (a, c), pristine (b, d) and APMS modified (c, e) AAO templates

on the templates surface. A minor difference displayed in phase image (Fig .S2) of the pristine and APMS modified templates may yield the same conclusion. The vibration intensity of APMS modified template subtracted the intensity of pristine one shows peak at 1593 cm^{-1} attributed to N-H deformation vibration in-plane (Fig. 3b). [56] When PVDF nanowires are embeded in the template nanopores, the N-H vibration shifts to 1650cm^{-1} with low frequency. It can be explained by the hydrogen bonds formed between the amino groups on modified template pores surface and fluorine atoms on PVDF chains. Nitrogen atoms on NH_2 groups have weaker attraction towards hydrogen atoms, due to lower electronegativity compared with oxygen atoms on hydroxyl groups. It results in stronger interaction between the hydrogen atoms on NH_2 groups and fluorine atoms on PVDF chains. [57] So the interactions between the functional groups and PVDF chains in nanopores of APMS modified templates are stronger than the interactions in pristine templates. The more hydrogen bonds and stronger interactions than the pristine template improve the polar phase content of PVDF nanowires. After APMS treatment, the surface of templates become less hydrophilic as displayed in the result of contact angle measurements (Fig. 4c). So the APMS treatment does not increase the polarity of the templates surface. In summary, more interaction points and stronger interaction enhance the polar phase of PVDF nanostructures, rather than the high polarity of nanopores surface.

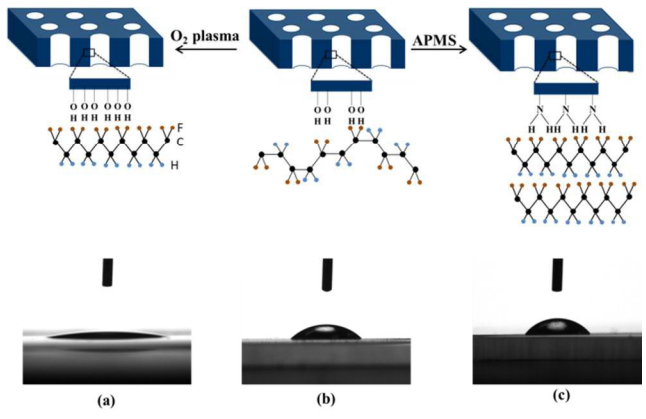

Figure 5 The contact angle measurements of water droplet deposited on the surface of oxygen plasma treatment (a), pristine (b) and APMS modified (c) AAO templates and corresponding schematic diagram of the polar phase formation. (Hydrogen, fluorine and carbon atoms are represented by blue, yellow and black spheres)

The TGA tests verify the induction effect of templates nanopores surface on polar phase. The first weight loss at about 200ºC observed at TGA curve of O_2 plasma treatment template, can be attributed to surface dehydration and loss of the incorporated OH^- and O^{2-} groups (Fig. 6a). The weight loss at approximately 550ºC is due to decomposition and total loss of the aminopropyl groups [58] from the APMS modified template. It is based on the fact that there is almost no significant weight loss in the AAO templates over this same temperature range. This further confirms that the aminopropyl groups are chemically bonded to the internal surface of the AAO template and are relatively thermally stable. The TGA curves of nanowires forming in different templates are represented by the curves of nanowires filled in different templates subtracted the curves of respective templates (Fig .6b). As reported, the weight loss of pure PVDF takes place at about 450ºC. [59] The weight loss at 70-100ºC is observed on the subtracted curve of nanowires in O_2 plasma treated templates. A weight loss happens between 70 and 100ºC is associated with the loss of the OH^- and O^{2-} groups. Due to the interaction between the OH groups on nanopores surface

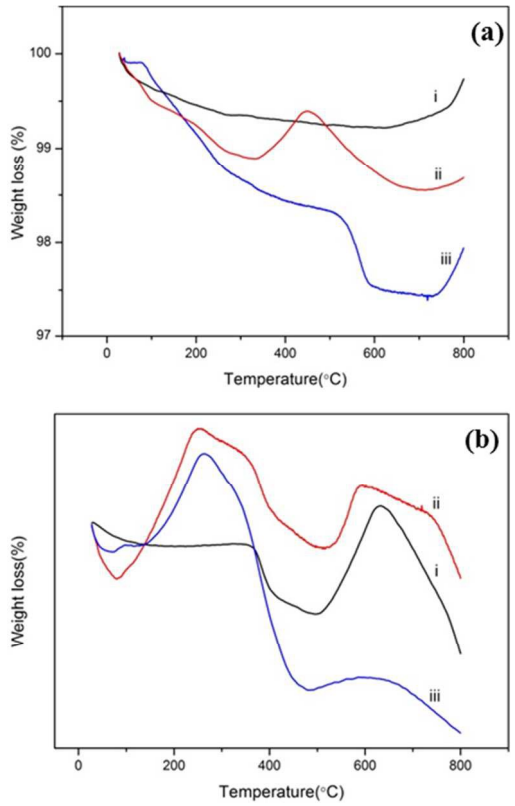

Figure 6 TGA curves of pristine (i), oxygen plasma treatment (ii) and APMS modified (iii) AAO templates (a); nanowires filled in pristine (i), oxygen plasma treatment (ii), and APMS modified (iii) AAO templates subtracted the curves of respective templates (c).

and PVDF nanowires, the thermally stable of OH groups decreases. Thereby the degradation temperature of OH groups is lower compared with the groups on template. In the same way, the interaction between the NH_2 groups and PVDF would results in a decrease of degradation temperature of aminopropyl groups. The weight loss of aminopropyl groups may overlap with the decomposition of PVDF nanowires therefore it exhibits a resulting curve as the Fig .6c(iii) shown.

Conclusion

The PVDF nanowires were fabricated by solution wetting AAO templates method. When the crystallization temperature increased, the polar phase content decreased obviously. The effect of drying temperature is stronger than solution concentration, which is consistent with the bulk film crystallized from solution. The polar solvent at low temperature and the hydroxyl groups on template nanopores surface both have an induction effect on the polar phase content of PVDF nanowires fabricated by pristine templates. The PVDF nanowires prepared by oxygen plasma modified templates show much more β phase even though the total amount of polar phase content was relatively constant. The high polarity of template surface reinforces the absorption between the templates nanopores surface and PVDF molecules. The TG^+ and TG^- conformation defects reduce dramatically due to the regular arrangement among hydroxyl groups. The polar phase content of PVDF nanowires increased from 40% prepared by the pristine template to 71% by the APMS modified template. More interaction points and stronger interaction enhance the polar phase of PVDF nanostructures effectively, rather than the high polarity of nanopores surface. This work may aid the design and fabrication of piezoelectric polymer nanodevices with well-defined structure and properties.

Acknowledgements

This work was supported by the National Science Foundation for Young Scientists of China (21504091).

Notes and references

[a] Lab of Polymer Composites Engineering, Changchun Institute of Applied Chemistry,Chinese Academy of Sciences, Changchun 130022, China.
E-mail: ranxh@ciac.jl.cn;
Fax: +86 431 85262424; Tel: +86 431 85262677
[b] University of Chinese Academy of Sciences, Beijing 100049, China

1. C. Bowen, H. Kim, P. Weaver and S. Dunn, *Energy & Environmental Science*, 2014, **7**, 25-44.
2. D. Mao, B. E. Gnade and M. A. Quevedo-Lopez, *Ferroelectric Properties and Polarization Switching Kinetic of poly (vinylidene fluoride-trifluoroethylene) Copolymer*, INTECH Open Access Publisher, 2011.
3. F. Guan, J. Wang, J. Pan, Q. Wang and L. Zhu, *Macromolecules*, 2010, **43**, 6739-6748.
4. L. Yang, X. Li, E. Allahyarov, P. L. Taylor, Q. Zhang and L. Zhu, *Polymer*, 2013, **54**, 1709-1728.
5. M. Steinhart, J. Wendorff, A. Greiner, R. Wehrspohn, K. Nielsch, J. Schilling, J. Choi and U. Gösele, *Science*, 2002, **296**, 1997-1997.
6. M. Raoufi and H. Schönherr, *RSC Advances*, 2013, **3**, 13429-13436.
7. S. Schlitt, A. Greiner and J. H. Wendorff, *Macromolecules*, 2008, **41**, 3228-3234.
8. Z. Hu and A. M. Jonas, *Soft Matter*, 2010, **6**, 21-28.
9. Z. Hu, G. Baralia, V. Bayot, J.-F. Gohy and A. M. Jonas, *Nano letters*, 2005, **5**, 1738-1743.
10. P. Huang, L. Zhu, Y. Guo, Q. Ge, A. J. Jing, W. Y. Chen, R. P. Quirk, S. Z. Cheng, E. L. Thomas and B. Lotz, *Macromolecules*, 2004, **37**, 3689-3698.
11. P. Huang, Y. Guo, R. P. Quirk, J. Ruan, B. Lotz, E. L. Thomas, B. S. Hsiao, C. A. Avila-Orta, I. Sics and S. Z. Cheng, *Polymer*, 2006, **47**, 5457-5466.
12. B.-S. Lee, B. Park, H.-S. Yang, J. W. Han, C. Choong, J. Bae, K. Lee, W.-R. Yu, U. Jeong and U.-I. Chung, *ACS applied materials & interfaces*, 2014, **6**, 3520-3527.
13. T. Lei, X. Cai, X. Wang, L. Yu, X. Hu, G. Zheng, W. Lv, L. Wang, D. Wu and D. Sun, *RSC Advances*, 2013, **3**, 24952-24958.
14. H. Shao, J. Fang, H. Wang and T. Lin, *RSC Advances*, 2015.
15. M. Kanik, O. Aktas, H. S. Sen, E. Durgun and M. Bayindir, *ACS nano*, 2014, **8**, 9311-9323.
16. R. A. Whiter, V. Narayan and S. Kar‐Narayan, *Advanced Energy Materials*, 2014, **4**, 1400519.
17. X. Z. Chen, Q. Li, X. Chen, X. Guo, H. X. Ge, Y. Liu and Q. D. Shen, *Advanced Functional Materials*, 2013, **23**, 3124-3129.
18. Z. Hu, M. Tian, B. Nysten and A. M. Jonas, *Nature materials*, 2009, **8**, 62-67.
19. X. Li, Y.-F. Lim, K. Yao, F. E. H. Tay and K. H. Seah, *Physical Chemistry Chemical Physics*, 2013, **15**, 515-520.
20. R. Hasegawa, Y. Takahashi, Y. Chatani and H. Tadokoro, *Polymer Journal*, 1972, **3**, 600-610.

21. X. He and K. Yao, *Applied physics letters*, 2006, **89**, 112909.
22. Y. Wu, Q. Gu, G. Ding, F. Tong, Z. Hu and A. M. Jonas, *ACS Macro Letters*, 2013, **2**, 535-538.
23. V. Cauda, S. Stassi, K. Bejtka and G. Canavese, *ACS applied materials & interfaces*, 2013, **5**, 6430-6437.
24. S. Oh, Y. Kim, Y. Y. Choi, D. Kim, H. Choi and K. No, *Advanced Materials*, 2012, **24**, 5708-5712.
25. N. Shingne, M. Geuss, B. Hartmann-Azanza, M. Steinhart and T. Thurn-Albrecht, *Polymer*, 2013, **54**, 2737-2744.
26. J. L. Lutkenhaus, K. McEnnis, A. Serghei and T. P. Russell, *Macromolecules*, 2010, **43**, 3844-3850.
27. K. Koga and H. Ohigashi, *Journal of applied physics*, 1986, **59**, 2142-2150.
28. M. Steinhart, P. Göring, H. Dernaika, M. Prabhukaran, U. Gösele, E. Hempel and T. Thurn-Albrecht, *Physical review letters*, 2006, **97**, 027801.
29. M. Steinhart, S. Senz, R. B. Wehrspohn, U. Gösele and J. H. Wendorff, *Macromolecules*, 2003, **36**, 3646-3651.
30. V. Cauda, B. Torre, A. Falqui, G. Canavese, S. Stassi, T. Bein and M. Pizzi, *Chemistry of Materials*, 2012, **24**, 4215-4221.
31. M.-C. García-Gutiérrez, A. Linares, J. J. Hernández, D. R. Rueda, T. A. Ezquerra, P. Poza and R. J. Davies, *Nano letters*, 2010, **10**, 1472-1476.
32. X. Li, Y.-F. Lim, K. Yao, F. E. H. Tay and K. H. Seah, *Chemistry of Materials*, 2013, **25**, 524-529.
33. D. Kim, S. Hong, J. Hong, Y. Y. Choi, J. Kim, M. Park, T. h. Sung and K. No, *Journal of Applied Polymer Science*, 2013, **130**, 3842-3848.
34. M. Pasquali, J. Liang and S. Shivkumar, *Nanotechnology*, 2011, **22**, 375605.
35. H. Wu, Z. Su and A. Takahara, *Soft Matter*, 2012, **8**, 3180-3184.
36. M. Kobayashi, K. Tashiro and H. Tadokoro, *Macromolecules*, 1975, **8**, 158-171.
37. A. Salimi and A. Yousefi, *Journal of Polymer Science Part B: Polymer Physics*, 2004, **42**, 3487-3495.
38. R. Gregorio, *Journal of Applied Polymer Science*, 2006, **100**, 3272-3279.
39. P. Martins, A. Lopes and S. Lanceros-Mendez, *Progress in polymer science*, 2014, **39**, 683-706.
40. R. Gregorio Jr and E. Ueno, *Journal of Materials Science*, 1999, **34**, 4489-4500.
41. R. Gregorio and D. S. Borges, *Polymer*, 2008, **49**, 4009-4016.
42. D. L. Chinaglia, R. Gregorio, J. C. Stefanello, R. A. Pisani Altafim, W. Wirges, F. Wang and R. Gerhard, *Journal of applied polymer science*, 2010, **116**, 785-791.
43. W. Ma, J. Zhang and X. Wang, *Journal of Materials Science*, 2008, **43**, 398-401.
44. W. Ma, J. Zhang and X. Wang, *Applied Surface Science*, 2008, **254**, 2947-2954.
45. R. Gregorio Jr and M. Cestari, *Journal of Polymer Science Part B: Polymer Physics*, 1994, **32**, 859-870.
46. A. A. Tsyganenko and P. P. Mardilovich, *J. Chem. Soc., Faraday Trans.*, 1996, **92**, 4843-4852.
47. U. Gedde, *Polymer physics*, Springer Science & Business Media, 1995.
48. M. Bohlén and K. Bolton, *Physical Chemistry Chemical Physics*, 2014, **16**, 12929-12939.
49. W. Wang, H. Fan and Y. Ye, *Polymer*, 2010, **51**, 3575-3581.
50. J. S. Meena, M.-C. Chu, Y.-C. Chang, H.-C. You, R. Singh, P.-T. Liu, H.-P. D. Shieh, F.-C. Chang and F.-H. Ko, *Journal of Materials Chemistry C*, 2013, **1**, 6613-6622.
51. Y. Wan, X. Qu, J. Lu, C. Zhu, L. Wan, J. Yang, J. Bei and S. Wang, *Biomaterials*, 2004, **25**, 4777-4783.
52. K. Kim, K. Lee, K. Cho and C. Park, *Journal of Membrane Science*, 2002, **199**, 135-145.
53. S. Bhattacharya, A. Datta, J. M. Berg and S. Gangopadhyay, *Microelectromechanical Systems, Journal of*, 2005, **14**, 590-597.
54. D. Losic and A. Santos, *Nanoporous Alumina: Fabrication, Structure, Properties and Applications*, Springer, 2015.
55. R. Qian, J. Yu, C. Wu, X. Zhai and P. Jiang, *RSC Advances*, 2013, **3**, 17373-17379.
56. W. W. Simons, *Sadtler handbook of infrared spectra*, 1978.
57. G. A. Jeffrey and G. A. Jeffrey, *An introduction to hydrogen bonding*, Oxford university press New York, 1997.
58. Z. Luan, J. A. Fournier, J. B. Wooten and D. E. Miser, *Microporous and Mesoporous Materials*, 2005, **83**, 150-158.
59. P. Mishra and K. Balasubramanian, *RSC Adv.*, 2014, **4**, 53291-53296.